

Ion Condensation onto Ribozyme is Site-Specific and Fold-Dependent

Naoto Hori,¹ Natalia A. Denesyuk,² and D. Thirumalai^{1,*}

¹*Department of Chemistry, University of Texas, Austin, Texas 78712, USA*

²*Biophysics Program, Institute for Physical Science and Technology,
University of Maryland, College Park, Maryland 20742, USA*

(Dated: February 18, 2019)

Abstract

The highly charged RNA molecules, with each phosphate carrying a single negative charge, cannot fold into well-defined architectures with tertiary interactions, in the absence of ions. For ribozymes, divalent cations are known to be more efficient than monovalent ions in driving them to a compact state although often Mg^{2+} ions are needed for catalytic activity. Therefore, how ions interact with RNA is relevant in understanding RNA folding. It is often thought that most of the ions are territorially and non-specifically bound to the RNA, as predicted by the counterion condensation (CIC) theory. Here, we show using simulations of *Azoarcus* ribozyme, based on an accurate coarse-grained Three Site Interaction (TIS) model, with explicit divalent and monovalent cations, that ion condensation is highly specific and depends on the nucleotide position. The regions with high coordination between the phosphate groups and the divalent cations are discernible at very low concentrations when the ribozyme does not form tertiary interactions. Surprisingly, these regions also contain the secondary structural elements that nucleate subsequently in the self-assembly of RNA, implying that ion condensation is determined by the architecture of the folded state. These results are in sharp contrast to interactions of ions (monovalent and divalent) with rigid charged rods in which ion condensation is uniform and position independent. The differences are explained in terms of the dramatic non-monotonic shape fluctuations in the ribozyme as it folds with increasing Mg^{2+} or Ca^{2+} concentration.

* dave.thirumalai@gmail.com

INTRODUCTION

RNA molecules are negatively charged polyelectrolytes (PEs) with each molecule carrying a total charge equal to $-Ne$ where N is the number of nucleotides and e is the elementary charge. The negative charges are localized on the phosphate groups. Because of the large electrostatic repulsion between the phosphate groups, RNA can only fold if the effective charge on the phosphate group is reduced or renormalized, which we know occurs by the counter ion condensation (CIC) mechanism [1–4]. In this process, described decades ago in remarkable studies by Oosawa and Manning [1, 2], the condensed ions are localized in an apparent volume occupied by the PE or any highly charged macroion. As a consequence, the effective charge on the negatively charged moieties in the PE (or the phosphate groups in DNA and RNA) is reduced from $-e$ to $-\beta e$ with $\beta < 1$ [1–3]. The renormalized charge parameter, β , can be calculated for PEs with regular shapes [3]. For example, the condition for ion condensation for a rod-like macroion is determined by the Manning parameter $\xi = \ell_B/b > 1/|z|$, where ℓ_B is the Bjerrum length, b is the mean distance between charges on the polyelectrolyte, and z is the valence of the counterion. The Bjerrum length is the distance at which the electrostatic energy of two univalent charges is equal to the thermal energy, $\ell_B = e^2 (4\pi\epsilon_0\epsilon k_B T)^{-1}$, where ϵ_0 is the vacuum permittivity, ϵ is the dielectric constant of the solvent, and $k_B T$ is the thermal energy. For highly charged rods, ion condensation occurs when $\xi \geq 1/|z|$, with the transition being sharp for long thin rods (high aspect ratio). A similar condition may be obtained for spherical macroions. In this case ion condensation does occur with a fraction localized in the vicinity of the sphere, but unlike the situation of the cylindrical macroion, there is not critical value of the ξ at which counterion condensation is initiated [3].

There are two implications of these well known aspects of the CIC theory summarized above that are relevant to the current study. (1) Monovalent ions ($|z| = 1$) are not as efficient in charge renormalization as higher valent ions ($|z| > 1$). Based on this consideration, we calculated that about 90% of the phosphate charge in *Tetrahymena* ribozyme is neutralized in the presence of divalent and trivalent cations [5]. (2) The condensation mechanism depends critically on the shape of the macroion. As noted above, the theoretical predictions are different for spheres and rods. Therefore, we expect that the CIC mechanism ought to be different for RNA, which undergoes substantial shape fluctuations during the ion-driven

folding process. The shape of *Azoarcus* ribozyme that is used as an example here, changes as the concentration of ions (Mg^{2+}) is increased from a low to a high value. This ribozyme, and many other RNA molecules, are not spherical even when folded [6]. Moreover, even at low Mg^{2+} concentrations, *Azoarcus* ribozyme does not adopt globally cylindrical structures although individual helices may be rigid enough to be pictured as small cylinders.

Because of the irregular shapes of RNA molecules at all ion concentrations ion-RNA interactions, which are often thought to involve diffuse ions that are territorially (within a volume of RNA where the electrostatic potential is substantial) but non-specifically bound require scrutiny. Motivated by the considerations described above, we answer the following questions here: How does CIC occur in such molecules whose shapes are not only irregular but also change as they fold? We are able to quantitatively answer this question because of the development of an accurate coarse-grained force field, which has been used to quantitatively predict the thermodynamic properties of *Azoarcus* ribozyme and other RNA molecules [7] in the presence of K^+ , Mg^{2+} and Ca^{2+} .

There is an additional reason for undertaking this investigation. The physically appealing CIC mechanism qualitatively explains RNA folding both from the stability and kinetic perspective [5]. The mechanism is based on the basic assumption that condensed ions are diffuse and freely move within the volume surrounding the RNA where the electrostatic potential is the largest. Indeed, the condition for ion condensation is obtained by assuming that the mobile but bound ions are in equilibrium with free ions (the chemical potential of these two species are identical) that explore the region outside the sphere of influence of the macroion [3]. Such an assumption does qualitatively explain the success of even the z -dependent folding kinetics of *Tetrahymena* ribozyme [8, 9]. However, our recent studies [7] suggest that the assumption of uniform condensation, often made in rationalizing electrostatic effects in RNA, may be qualitatively incorrect. In other words, nucleotide specific interaction between ions (especially Ca^{2+} and Mg^{2+} ions) provide the key in quantitatively describing charge renormalization in ribozyme folding.

In order to fully understand the nature and consequence of ion condensation onto RNA, we undertook two types of simulations. We first probed the interaction of divalent cations with small finite-sized rigid rods of different linear charge density, expressed as $b = n/L$ where n is the total number of charges and L is the cylinder length. It follows that b is the mean distance between charges. However, in our simulations the distance between the charges

(*b*) is a constant. We also investigated the condensation of divalent cations onto *Azoarcus* ribozyme using an accurate model introduced recently [7]. By comparing the results of these two systems, we elaborate on the importance of the architecture of the macroion (rod versus ribozyme) on the ion condensation mechanism. Our major finding is that the shape of the RNA matters for counterion condensation. In other words, ion-condensation to RNA depends exquisitely on the folded RNA architecture, and hence cannot be treated as a non-specific interaction that is used to understand CIC for macroion with definite simple shapes. A surprise in our study is that the specificity of ion binding plays a vital role in driving RNA folding even at very low divalent ion concentrations.

MODEL AND METHODS

Rigid rod simulations: A 5 nm-long rigid cylindrical rod is placed at the center of 15 nm-wide cubic box (Fig. 1a and b). The diameter of the rod is 0.42 nm, which is the size of the phosphate bead in the coarse grained RNA model described below. Technically, the rod is constructed by overlapping spheres that are separated by 0.1 nm. The rod is completely rigid and fixed at the center of the simulation box, whereas ions are allowed to move freely around the rod. We use periodic boundary conditions. Three different charge densities on the rod, $\rho_{1D} = -1, -2,$ and $-5 e \text{ nm}^{-1}$ were simulated, which translates to the constant separation distance (*b*) between neighboring charges as 1.0, 0.5, and 0.2 nm, respectively. For comparison, the Bjerrum length (ℓ_B) is 0.73 nm at the simulation temperature, $T = 37^\circ\text{C}$. The interactions between the charges on the rod and the ion are the same as in the coarse-grained RNA-ion model [7]. Ions ($\text{K}^+, \text{Cl}^-,$ and Mg^{2+}) are modeled as spheres and interact with each other and with the charged rod via the excluded volume potential, which is identical to the one used in the RNA model,

$$U_{\text{Ex}} = \varepsilon_{ij} \left[\left(\frac{1.6}{r_{ij} + 1.6 - D_{ij}} \right)^{12} - 2 \left(\frac{1.6}{r_{ij} + 1.6 - D_{ij}} \right)^6 + 1 \right], \quad r_{ij} \leq D_{ij} \quad (1)$$

where r is the distance of the two beads, $D_{ij} = R_i + R_j$ and $\varepsilon_{ij} = \sqrt{\varepsilon_i \varepsilon_j}$. The values of R_i and ε_i for the ions and the RNA sites are tabulated in Table S1 in the Supplementary Information (SI). The R_i and ε for the charged rod is the same as the phosphate site in the RNA model. If $r_{ij} > D_{ij}$ then $U_{\text{EX}} = 0$. For any pair of charged beads, the standard

Coulomb potential is used,

$$U_{\text{Ele}} = \frac{q_i q_j}{4\pi\epsilon_0\epsilon r_{ij}} \quad (2)$$

where q_i is the charge of the i^{th} bead. The dielectric constant, ϵ , is temperature dependent and is 74 at the simulation temperature $T = 37^\circ\text{C}$. A series of Langevin dynamics simulations were performed for 2×10^7 iteration time steps, in which ion positions are saved every 100 steps. Thus, in total 2×10^6 snapshots are used for analyses for each setup.

We ought to emphasize that the results of rigid rod simulations for different purposes have been reported numerous times in the literature (see for example [10–12]) although new phenomena continue to be found in [13]. The simulations presented here merely serve as a control in order to illustrate the dramatically different findings for the *Azoarcus* ribozyme.

Simulations of group I intron RNA: Because the model and simulation methods of the ribozyme were described in detail previously [7], we give only a brief description here. We used a coarse-grained Three Interaction Site (TIS) RNA model that has three interaction sites, for each nucleotide, corresponding to phosphate, sugar and base moieties [14]. All the ions are explicitly treated whereas water is modeled implicitly using the temperature-dependent dielectric constant. We considered concentration of Mg^{2+} ions in the range from 0 to 30 mM in the presence of either 50 mM or 12 mM of K^+ that is typically used in the Tris buffer [15]. We added an appropriate number of anions (Cl^-) to ensure that neutralize the entire system is charge neutral. We performed a series of Langevin dynamics simulations at 37°C in order to efficiently sample conformations of the system containing the ribozyme and ions [16]. All the simulations were conducted using a periodic-boundary cubic box with each side being 35 nm.

The crystal structure of *Azoarcus* group I intron (PDB 1U6B [17], Fig. 1c and d) was used as the reference structure for the native conformation. For convenience, we assign nucleotide numbers from 1 through 196 to the sequence, which is conventionally numbered from 12 to 207 in the *Azoarcus* group I intron literature [17].

Data analyses: To quantify ion condensation onto the RNA and the rigid rod, we calculated the *local ion concentration*, a fingerprint of ion interaction with the macroion, around the i^{th} phosphate (or point charges on the rod) defined as,

$$c_i^* = \frac{1}{N_A V_c} \int_0^{r_c} \rho_i(r) 4\pi r^2 dr, \quad (3)$$

where $\rho_i(r)$ is the number of ions per unit volume (number density) of the ion at the distance r from the i^{th} phosphate, V_c is the spherical volume of radius r_c , N_A is the Avogadro's number to represent c_i^* in molar units. We use the Bjerrum length as the cutoff distance, $r_c = \ell_B = 0.73$ nm because at that distance the favorable Coulomb attraction between a cation and an anion ($z = 1$) is $k_B T$.

We also calculated the fluctuations in the local ion concentration as the normalized root-mean-square deviation from the mean,

$$\Delta c_i^* = \frac{\langle (c_i^* - \langle c_i^* \rangle)^2 \rangle^{1/2}}{\langle c_i^* \rangle}, \quad (4)$$

where $\langle c_i^* \rangle$ is the ensemble average of the local ion concentration around the i^{th} nucleotide. Thus, $c_i^* - \langle c_i^* \rangle$ is an instantaneous deviation from the ensemble average. The average ion concentration is,

$$\overline{\langle c^* \rangle} = \frac{1}{N} \sum_{i=1}^N \langle c_i^* \rangle, \quad (5)$$

where N is the number of nucleotides. Note that the upper bar indicates an average over the sequence, whereas the bracket indicates the ensemble average. The extent of deviation of ion concentration fluctuation from $\langle c^* \rangle$ along the sequence was calculated using,

$$\sigma^2 = \frac{1}{N} \sum_{i=1}^N \left(\langle c_i^* \rangle - \overline{\langle c^* \rangle} \right)^2. \quad (6)$$

In the results section, for simplicity, we omit the brackets for the ensemble average. Thus, all quantities are averaged over an ensemble of configurations in the system (ions and the charged RNA or the rod) unless otherwise stated.

For charged rods, we also computed the total charge per unit length due to contributions from each ionic species. The effective charge densities around the rod was calculated as the amount of accumulated charge per unit length for the ion species m ,

$$Q_m(R) = z_m \int_0^R \rho_m(R') 2\pi R' dR', \quad (7)$$

where $\rho_m(R)$ is the number density of species m at the radial distance R from the axis of the cylinder, and z_m is its valence. Note that Q can be computed for each ion Mg^{2+} , K^+ , and Cl^- independently. Finally, the total effective charge per unit length is the sum of the rod charge and contributions from those ions,

$$Q_T(R) = \rho_{\text{1D}} + Q_{\text{Mg}^{2+}}(R) + Q_{\text{K}^+}(R) + Q_{\text{Cl}^-}(R). \quad (8)$$

Note that we use R for the radial distance from the center of the rods in the cylindrical coordinate, whereas r is for the distance from the point charges on the rod in the spherical coordinate (see Fig. 1a).

RESULTS

Charged cylindrical rods: We first describe condensation of ions onto charged rods with varying spacing between fixed charges, $b = -e/\rho_{1D}$, where ρ_{1D} is the charge density of the rod. Based on the CIC theory, we expect that ions should condense uniformly along the rod. The condition for condensation in the CIC theory is that $\xi > 1/|z|$, where z is the valence of the ion species. In the absence of multivalent salt, $\xi > 1$ and thus we expect ions should condense on rods when $\rho_{1D} = -5 e/\text{nm}$ ($\xi = 3.6$) and $\rho_{1D} = -2 e/\text{nm}$ ($\xi = 1.5$) among the three values of charge densities we examine here. This expectation is borne out in the simulations even though the aspect ratio (≈ 11.9) is relatively small. In Fig. 2(a-c), the cumulative charges, Q (Eq. 7), around the rod are plotted for each ion species and the net charge. The condensation of monovalent ions appears as a sharp increase in Q_{K^+} around the vicinity of the rod ($R \sim 5 \text{ nm}$), with a subsequent reduction of the net negative charge at longer distances (thick lines in gray). The amount of condensation is larger for the rod with $\rho_{1D} = -5 e/\text{nm}$ than for one with $\rho_{1D} = -2 e/\text{nm}$. In the case of the lowest charge density ($-1 e/\text{nm}$ corresponding $\xi = 0.7$), condensation is not observed as predicted by the CIC theory (Fig. 2c).

The condition for condensation, $\xi > 1/|z|$, also implies that the charged rod must be surrounded to a greater degree by Mg^{2+} than K^+ . This prediction is also borne out in the simulations. In Fig. 2 (d and e), Mg^{2+} ions condense in the immediate vicinity of the rods taking over the role of K^+ in the charge renormalization. The replacement of K^+ by Mg^{2+} in the vicinity of the rod is expected based on the counterion release mechanism (leads to an entropy of the whole system increase), which is another well known consequence of the CIC theory. The condensation of cations, and the subsequent net reduction of negative charge on the rod, are more efficient in the presence of Mg^{2+} than when $z = 1$ (compare panels (a) and (d) in Fig. 2). Since the condensation condition for Mg^{2+} is $\xi > 0.5$, a distinct increase of $Q_{\text{Mg}^{2+}}$ is visible even at the lowest density case, $\rho_{1D} = -1 e/\text{nm}$ ($\xi = 0.7$) albeit the extent of condensation is not as great as found in the two rod systems with higher density

(Fig. 2f).

The results quoted above using the control simulations are entirely in accord with the CIC theory predictions. The extremely close correspondence between the CIC theory and simulations for charged rods motivated us to make several assessments of ion condensation phenomena in ribozyme folding, in which we use the same explicit-ion model. In order to make quantitative comparisons between the rod and RNA folding simulations, we need to devise a quantity to precisely measure the ion condensation. The radial distributions in the cylindrical coordinate is not suitable for flexible RNA chains whose the persistence length ($1 \sim 2$ nm for a single strand) and the Debye screening length (1.3 nm in the simulation conditions) are similar. With this in mind, we defined a local ion concentrations (c^*) and the associated fluctuations (Eqs. 3-4) in the spherical coordinate for each point charge. The results of the rod simulations in terms of c^* are shown in Fig. 3 (a and b) for the three rod charge densities in the presence of 5 mM MgCl_2 and 50 mM KCl . It is clear that the density of condensed ions around the charges in the rod is uniform; there is no position dependence along the rod. From panels (c) and (d) in Fig. 3, the fluctuation in c^* is the lowest in the case of Mg^{2+} condensed for the highest charge density rod. Both by lowering the linear charge density and reducing the valence of cations ($\text{Mg}^{2+} \rightarrow \text{K}^+$) make the condensed state is less favorable, thus increasing the magnitude of charge fluctuations. These quantitative descriptions for the charged rods set the stage for analyzing the completely contrasting behavior in ion-ribozyme interactions.

[Mg^{2+}]-dependent folding of *Azoarcus* ribozyme: Before proceeding to examine the roles of ions in RNA folding, we summarize briefly the [Mg^{2+}]-dependent folding of the *Azoarcus* ribozyme, which has been investigated in a previous study using an elaborate version of the TIS model [7]. The folding process of the ribozyme (Fig. 1) strongly depends on the concentration of Mg^{2+} . In Fig. 4a, the dependence of the radius of gyration (R_g) on [Mg^{2+}] is shown in gray lines for two different conditions of monovalent salt concentration, $[\text{K}^+] = 12$ and 50 mM. The global compaction of the RNA appears as a single transition in R_g occurring at $C_m \approx 1.5$ mM, where we designate C_m as the midpoint concentration of [Mg^{2+}] separating the folded and unfolded states. Comparison of 12 mM K^+ simulation data and SAXS experiments at the equivalent condition [15] (squares in Fig. 4) shows excellent agreement, thus establishing that our model captures monovalent- and divalent-ion dependence of folding of *Azoarcus* ribozyme (for additional details see [7]). In the rest part of this

paper, we report detailed analyses of ion distributions around the RNA. Comparison with interaction of divalent ions with highly charged rods illustrates the importance of ribozyme architecture on ion–RNA interactions.

Radial profiles of ion condensation: We calculated the density profiles of each ion species around phosphate, $\rho_i(r)$, where r is the distance from the phosphate of the i^{th} nucleotide. We also computed the profiles of phosphate–phosphate distance, which can be used to trace the compaction of the ribozyme. The ensemble-averaged profiles, for given Mg^{2+} concentration, are shown in Fig. 5. From the profiles of the phosphate (gray dotted lines in Fig. 5), we can track the folding of the ribozyme as follows. The peaks at $r \approx 0.55$ nm is roughly the distance between two consecutive phosphates, and the smaller second peak corresponds to the location of the second nearest-neighbor phosphates. The amplitudes of these two peaks do not show significant change as $[\text{Mg}^{2+}]$ increases. However, the folding process can be discerned by the increase in $\rho_p(r)$ in the range $0.7 < r < 0.9$ nm (red arrows in Fig. 5). At low $[\text{Mg}^{2+}]$, there is practically no density in ρ in this range ($\rho(r) \approx 0$). As $[\text{Mg}^{2+}]$ increases, we find that the amplitude increases, which shows that Mg^{2+} facilitates the approach of non-neighboring phosphates. The increase in $\rho(r)$ in this range coincides with the compaction of the ribozyme and subsequent folding as shown in Fig. 4(a).

In the absence of Mg^{2+} , K^+ cations are condensed around the ribozyme, regardless of the monovalent salt concentration, $[\text{KCl}] = 12$ mM or 50 mM (Figs. 5a and S1a). Under these conditions with $[\text{Mg}^{2+}] = 0$, all tertiary interactions are disrupted but helices, except P3 and P7, form secondary structures (Fig. 1c). Thus, K^+ cations must be condensed around the vicinity of phosphates to balance the electrostatic repulsion between negative charges on the phosphates. The distance to condensed K^+ , $r \approx 0.4$ nm, is closer than the neighboring phosphate. In the presence of Mg^{2+} , $\rho(r)$ for K^+ decreases dramatically as the Mg^{2+} concentration increases (Fig. 5 b-d). This shows, rather vividly, that K^+ ions condensed around RNA are replaced with Mg^{2+} ions because divalent cations screen negative charges on RNA more efficiently than monovalent cations. By replacing two K^+ ions by one Mg^{2+} , there is a net gain in translational entropy of the ions. This is the counterion release mechanism predicted by the CIC theory.

Fingerprint of local ion concentration c_i^* : In order to examine the relationship between ion condensation and Mg^{2+} -driven RNA folding, we calculated the local ion con-

centration of the i^{th} nucleotide c_i^* (Eq. 3). The cutoff distance to define the local volume is chosen to be the Bjerrum length, $r_c = 0.73$ nm. The range of this distance covers the peaks in the radial distributions of both K^+ and Mg^{2+} (Fig. 5). Accordingly, c_i^* is expected to capture the amount of ion atmosphere around each nucleotide, and such a fingerprint is dependent on the architecture of the folded state of the RNA. The overall ion condensation of the entire molecule, $\overline{c^*}$, is calculated as the average of the local ion concentration along the RNA sequence (Eq. 5, see Models and Methods).

The changes in $\overline{c^*}$ as a function of $[\text{Mg}^{2+}]$ is shown in Fig. 4(b). As noted previously, more K^+ cations condense at lower Mg^{2+} than at higher Mg^{2+} concentrations. Indeed, $\overline{c_{\text{K}^+}^*}$ monotonically decreases as $[\text{Mg}^{2+}]$ increases (green lines). The folding midpoint of Mg^{2+} concentration is around 1.5 mM. Above the midpoint, Mg^{2+} ions are more dominantly found in the vicinity of the RNA than K^+ . $\overline{c_{\text{Mg}^{2+}}^*}$ does not vary significantly as a function of K^+ concentrations for the entire range of $[\text{Mg}^{2+}]$ (Fig. 4b, solid line for $[\text{K}^+] = 50$ mM and dotted line for 12 mM). The sharp increase in $\overline{c_{\text{Mg}^{2+}}^*}$ is well correlated with the global compaction of the ribozyme, that is evident as the decrease in R_g in Fig. 4(a).

Ion condensation is site-specific: In Fig. 4c, we show variances, σ^2 , of the local ion concentration over the RNA sequence (Eq. 6). This quantity indicates how much of each ion species are localized at particular positions along the sequence for each solution condition. As Mg^{2+} concentration increases, σ^2 for K^+ monotonically decreases, although it is much smaller compared to divalent cations for the entire range of $[\text{Mg}^{2+}]$. This means that Mg^{2+} ions tend to be localized at specific positions more than K^+ ions. In particular, σ^2 for Mg^{2+} sharply increases reaching a maximum around $[\text{Mg}^{2+}] \approx 3$ mM. This is because Mg^{2+} ions are preferentially localized to specific places, which are, surprisingly, determined by the tertiary structure of the ribozyme. Beyond the midpoint C_m , the value of σ^2 decreases modestly because the specific sites of higher phosphate densities are being occupied by existing localized Mg^{2+} . The newly added Mg^{2+} ions start contributing to lessen the gap between specific and other non-specific sites.

Fig. 6 shows the distributions of the local ion concentration along the RNA sequence. This figure shows that all non-zero value of Mg^{2+} condensation is highly specific. The extent of condensation depends on the nucleotide. Even at the lowest $[\text{Mg}^{2+}] = 0.4$ mM (much less than C_m) there is a significant density of Mg^{2+} around $i \approx 115$, which covers the triple helix (TH) of *Azoarcus* ribozyme. A clear implication is that Mg^{2+} binding is highly

specific. More importantly, charge neutralization resulting in $\beta < 1$, occurs at the lowest $[\text{Mg}^{2+}]$ not uniformly, as predicted by the CIC theory, but occurs in a manner that initiates folding. This would mean that different regions of this ribozyme order at somewhat distinct Mg^{2+} concentration, as illustrated previously (see Fig. 2b in [7]). In other words, there is a distribution of $[\text{Mg}^{2+}]$ at which different domains achieve native structure with C_m being the mean reported by calculating of inferring a given folding order parameter.

In the absence or at low Mg^{2+} concentrations, the amount of condensed K^+ depends significantly on positions along the RNA sequence. At low Mg^{2+} concentrations, the ribozyme is unfolded with some helices intact. To see if there is any relationship between K^+ condensation and such residual structure, we compare the distribution of c^* with the fraction of secondary structure formation in Fig. 7(a). The profile of condensed K^+ (green in Fig. 7a) has several characteristic minima that correspond to loops in the stem-loop structures of P2, P5, P6, P8 and P9. This indicates that the distribution of K^+ reflects the shape of RNA that is mostly due to residual secondary structures at low $[\text{Mg}^{2+}]$.

At high Mg^{2+} concentration ($[\text{Mg}^{2+}] > 1.5 \text{ mM}$), the localization of condensed Mg^{2+} ions depends on the tertiary structures of the RNA (Fig. 6c and d). The local concentration of Mg^{2+} correlates with the local density of phosphates (compare blue and gray lines in Fig. 7b). Under such conditions, all the native secondary structures are formed with almost unit probability, but we do not find any secondary-structure dependence of condensed Mg^{2+} .

The relationship between ion condensation and local density of phosphates is vividly illustrated in Fig. 8(a, b). At low $[\text{Mg}^{2+}]$, the ribozyme is mostly unfolded, predominantly containing only secondary structures. Because there is no stable tertiary interactions, c_{P}^* values are small (Fig. 8a, horizontal axis. $c_{\text{P}}^* \approx 3 \text{ M}$). Accordingly, c^* for Mg^{2+} are relatively low and K^+ are predominantly condensed. However, there are six nucleotides that have higher c^* for both P and Mg^{2+} (see the rectangle of $c_{\text{P}}^* > 3.5 \text{ M}$ and $c_{\text{Mg}^{2+}}^* > 0.5 \text{ M}$ in Fig. 8a). We identified all those nucleotides to be ones involving the central triple helix (TH) formation; nucleotides 39, 40 and from 113 to 116. In accordance with the previous study [7], TH starts to form around $[\text{Mg}^{2+}] = 0.4 \text{ mM}$ ($< C_m$). The data in Fig. 8 indicates that there are Mg^{2+} ions specifically bound to the sites around TH. In contrast, at high $[\text{Mg}^{2+}]$, the entire ribozyme is folded and c_{P}^* can be as high as $\sim 7 \text{ M}$ depending on the local architecture (Fig. 8b). The amount of condensed Mg^{2+} is well correlated with the local concentration of phosphates. There is a weak anti-correlation between K^+ condensation and

local phosphate concentration.

Fluctuations of condensed ions: RNA folding is a stochastic process driven by thermal fluctuations and the solution conditions. Consequently, it would be interesting to see how these condensed ions fluctuates at different stages of folding. In Fig. S3, normalized fluctuations of the local ion concentrations, Δc^* (Eq. 4), for each nucleotide are shown for the several solution conditions. Below or around the midpoint Mg^{2+} concentration, where the ribozyme folding is not completed, fluctuations of condensed K^+ ions and Mg^{2+} have similar position dependence. This correlation is more clearly seen in the logarithm plot of Δc_{Mg}^* vs Δc_{K}^* in Fig. 8(c). Comparing Figs. 6 and S3, we also find that nucleotide positions that have high c^* values also have small Δc^* . This indicates that the specific positions, where more ions are condensed, bind those ions also more tightly. Once the ions reach the “equilibrium” positions, they tend to be localized.

The correlation between the fluctuations of Δc_{Mg}^* and Δc_{K}^* changes dramatically after the midpoint, $[\text{Mg}^{2+}] > 1.5 \text{ mM}$ (Fig. S3d and e). There is anti-correlation between $\log \Delta c_{\text{Mg}}^*$ and $\log \Delta c_{\text{K}}^*$ (Fig. 8d). As discussed in previous sections, there are specific positions where more Mg^{2+} ions are condensed (Fig. 6) beyond the midpoint of $[\text{Mg}^{2+}]$. At these positions, there are less fluctuations in c_{Mg}^* (smaller Δc_{Mg}^*) but higher fluctuations in c_{K}^* (larger Δc_{K}^*), reflecting strong condensation of Mg^{2+} .

Ion condensation in Calcium-driven folding: We have hitherto focused on the condensation of K^+ in the absence and presence of Mg^{2+} , and the condensation of Mg^{2+} itself. It is known that Ca^{2+} could also facilitate *Azoarcus* ribozyme folding although the folded state is not catalytically active and is modestly less compact than it is in the presence of Mg^{2+} [7, 15]. We repeated the same analyses in the case of Ca^{2+} -dependent folding instead of Mg^{2+} . Both average local concentration (\bar{c}^*) and its variance (σ^2) show similar trends as the case of Mg^{2+} (Fig. 4b and c). At higher solution concentration ($[\text{Mg}/\text{Ca}^{2+}] \gtrsim 1 \text{ mM}$), the amount of condensation given by \bar{c}^* is slightly less in the case of Ca^{2+} .

Fig. S4 shows the sequence dependence of the local concentration (c^*) and fluctuation (Δc^*) in the case of Ca^{2+} . Comparing them with Fig. 6 and S2, the condensation profiles of Ca^{2+} and K^+ bear remarkable resemblances to the Mg^{2+} case. At the highest concentration ($[\text{Mg}/\text{Ca}^{2+}] = 30 \text{ mM}$), the local concentration of Ca^{2+} has the same peak positions as Mg^{2+} , but has $\sim 20\%$ lower values. Comparison of the fingerprint of ion concentration profiles

between Mg^{2+} and Ca^{2+} clearly illustrates the efficacy of Mg^{2+} of creating a compact and functionally competent ribozyme.

DISCUSSION

The central result of this study is that the nature of ion condensation onto *Azoarcus* ribozyme differs drastically from theoretical predictions for regularly shaped polyanions. For example, the CIC theory shows that ions condense uniformly onto highly charged rods. The positively charged ions are localized at the position of the charges on the rod. In sharp contrast, in *Azoarcus* ribozyme, and presumably other RNA molecules as well, the condensation is highly non-uniform and nucleotide specific and critically depends on the structure of the RNA. We note in passing that the prevailing view in much of the RNA literature is that most of the ions are uniformly condensed onto RNA although crystal structures have shown that there are site specific localization of Mg^{2+} . A natural explanation of our finding is that the electrostatic potential around the phosphate groups is non-uniform but in the folded structure with tertiary interactions contains pockets of high negative potentials. Consequently, ions are specifically drawn, with higher probability, to regions of large negative electrostatic potential with smaller ions approaching these regions easily. Indeed, this was first shown in our previous study using coarse-grained and atomic detailed simulations (see Fig. S11 in [7]). However, what is surprising in this study is that the ions sense these regions even at low divalent ion concentrations, when there is no tertiary interaction present.

Link to the shape fluctuations in the ribozyme: The non-uniformity and site specific ion-RNA interactions can be succinctly illustrated by considering the ion concentration dependent changes in the shape parameters, asphericity Δ ($0 \leq \Delta \leq 1$) and prolateness S ($-0.25 \leq S \leq 2$) [18, 19], which are readily computed from the inertia tensor that is related to the square of the radius of gyration. For reference, it is worth pointing out both Δ and S are unity for rods, whereas $\Delta = S = 0$ for spheres. For long self-avoiding polymers numerical results show that $\Delta = 0.55$ and $S = 0.92$ (a prolate ellipsoid) [20]. In contrast to the values of the shape parameters for rods, the changes in $\langle \Delta \rangle$ and $\langle S \rangle$ as a function of $[\text{Mg}^{2+}]$ for the ribozyme, at the two values of K^+ concentration, exhibit unusual non-monotonic dependence, which is not reflected in R_g (inset in Fig. 9). This figure also shows the distributions $P(\Delta)$ and $P(S)$ at three Mg^{2+} concentrations. Surprisingly, the widths of $P(\Delta)$ and $P(S)$,

which depend non-monotonically on $[\text{Mg}^{2+}]$, are relatively large. Therefore, the ribozyme fluctuations are substantial. Two comments are worth making: (1) The values of Δ and S depend greatly on the K^+ concentration, which is also reflected in the R_g as a function of Mg^{2+} concentration. (2) The minimum in $\langle\Delta\rangle$ and $\langle S\rangle$ at $[\text{Mg}^{2+}] \approx 1.5$ mM, the midpoint of the folding transition, where the ribozyme almost resembles a sphere is interesting. At high and low Mg^{2+} concentrations, the values of $\langle\Delta\rangle$ show that globally the ribozyme may be pictured as a prolate ellipsoid. It also implies that this ribozyme and others are not as densely packed as proteins [6]. The irregular shape presented to the ions leads to the high specificity of ion-RNA interactions. It is likely that this finding would apply to any RNA molecules whose shape has grooves and whose surface is not regular. It is most interesting that there is a calculable fingerprint for ion-RNA interactions that is a reflection of the folded structure. A clear implication is that, even at very low ion concentration, binding is highly specific. This interpretation differs from the usual assertion that the stability of RNA is determined largely by diffuse divalent cations [21].

Flexible polyelectrolytes: Just as is the case for RNA, which does adopt a well-defined folded structure at high ion concentrations, the shapes of flexible PEs are also highly variable. Therefore, it follows that the CIC theory should not be quantitative in predicting the nature of ion condensation. Indeed, early simulations showed [22] that ion condensation is non-uniform in the presence of divalent and trivalent cations for PEs in poor solvents. Indeed, in certain cases the divalent cations and the monomers are packed as in a crystalline arrangement, which would be inconsistent with the CIC theory. Using theory, Muthukumar [23] has shown that, even in monovalent salts ($z=1$), the condensation process in flexible PEs is non-uniform and could be understood by the variations in the local dielectric mismatch. A more recent simulation study [24] has also arrived at the conclusion that the condensation of monovalent ions depends crucially on the shape of the PE. In particular, they showed that non-uniform condensation is determined by the molecular topology. Thus, the conclusion that shapes determine ion condensation holds for both synthetic PEs and RNA. The latter has additional features (for example stacking interactions and hydrogen bonding), which make RNA different from a synthetic. In particular, the ion-induced shape changes in PEs are not as spectacular as they are in RNA.

CONCLUSION

The Oosawa-Manning theory of ion condensation, which assumes that there is an equilibrium between bound and free ions, is the basis of our understanding of many thermodynamics properties of highly charged polyelectrolytes. As shown multiple times previously and in the simulations here the predictions of the CIC theory are quantitatively correct if the charged polyelectrolytes adopt regular shapes, such as rods and spheres. This is not the case in RNA, which although is a polyanion, does not adopt a simple shape but undergoes large conformational transitions as it folds. Our simulations of *Azoarcus* ribozyme in the presence of Mg^{2+} or Ca^{2+} in a buffer containing K^+ ions show that ion binding is highly specific. Surprisingly, the specificity of binding depends on the folded structure of the RNA. In other words, in this ribozyme with a complex fold, the charge neutralization of phosphates does not occur uniformly as predicted by CIC theory for rod-like macroions. There are specific regions where condensation occurs, even at very low concentrations of the divalent cations. Although we have arrived at this unexpected finding using simulations of one ribozyme, we expect that the main conclusion should be applicable for other RNA molecules.

We conclude with the following additional comments. (1) We find, perhaps not surprisingly, that monovalent ions unbind (termed as counterion release process) when RNA is titrated with divalent ions (Fig. 6). This validates one of the predictions of the CIC theory. The release of K^+ , however, occurs from specific nucleotide locations on the RNA, which is not anticipated in the CIC theory. (2) It is unclear to us if our findings, especially the exquisite specificity of the predicted nucleotide-dependent binding of ions to RNA, could be tested in experiments because of the highly correlated and many-body nature of ion condensation. Multi color FRET experiments may be used to label regions of high affinity for divalent cations. The conformational changes as a consequence of ion binding and unbinding at these location could be used, most likely in conjunction with simulations, to determine the architecture dependent interaction of ions with RNA. (3) Our results show that charge renormalization of phosphates, as might be surmised by the diffuse binding picture of ion-RNA interactions, but occurs in a highly heterogeneous manner. The fingerprints of ion localization show that the extent of charge neutralization depends on the nucleotide position – finding that has to be incorporated in calculating free energy changes of RNA as it folds. (4) The clear implication of our results is that even when using coarse grained models

ions should be modeled explicitly to reflect their sizes and charge densities. However, it is possible that electrostatic interactions due to monovalent ions can be accounted for by using effective interactions [25]. But in order to obtain accurate thermodynamics of RNA folding divalent ions have to be explicitly modeled [7, 26]

Acknowledgements: We thank Dr. Hung T. Nguyen for useful discussions. This work was supported by a grant from the National Science Foundation (CHE 16-36424) and the Welch Foundation (F-0019) through the Collie–Welch Chair.

-
- [1] F. Oosawa, “A simple theory of thermodynamic properties of polyelectrolyte solutions,” *J. Polym. Sci.* **23**, 421–430 (1957).
- [2] G. S. Manning, “Limiting laws and counterion condensation in polyelectrolyte solutions. I. colligative properties,” *J. Chem. Phys.* **51**, 924–933 (1969).
- [3] F. Oosawa, *Polyelectrolytes* (Marcel Dekker, 1971).
- [4] S. Alexander, P. Chaikin, P. Grant, G. Morales, P. Pincus, and D. Hone, “Charge renormalization, osmotic pressure, and bulk modulus of colloidal crystals: Theory,” *J. Chem. Phys.* **80**, 5776–5781 (1984).
- [5] S. L. Heilman-Miller, D. Thirumalai, and S. A. Woodson, “Role of counterion condensation in folding of the Tetrahymena ribozyme I. equilibrium stabilization by cations,” *J. Mol. Biol.* **306**, 1157–1166 (2001).
- [6] C. Hyeon, R. I. Dima, and D. Thirumalai, “Size, shape, and flexibility of RNA structures,” *J. Chem. Phys.* **125**, 194905–10 (2006).
- [7] N. A. Denesyuk and D. Thirumalai, “How do metal ions direct ribozyme folding?” *Nature Chem.* **7**, 793–801 (2015).
- [8] S. L. Heilman-Miller, J. Pan, D. Thirumalai, and S. A. Woodson, “Role of counterion condensation in folding of the Tetrahymena ribozyme II. counterion-dependence of folding kinetics,” *J. Mol. Biol.* **309**, 57–68 (2001).
- [9] D. Thirumalai, N. Lee, S. A. Woodson, and D. Klimov, “Early events in RNA folding,” *Annu. Rev. Phys. Chem.* **52**, 751–762 (2001).
- [10] N. Grønbech-Jensen, R. J. Mashl, R. F. Bruinsma, and W. M. Gelbart, “Counterion-induced attraction between rigid polyelectrolytes,” *Phys. Rev. Lett.* **78**, 2477–2480 (1997).
- [11] I. Borukhov, D. Andelman, and H. Orland, “Steric effects in electrolytes: A modified Poisson–Boltzmann equation,” *Phys. Rev. Lett.* **79**, 435 (1997).
- [12] M. Deserno, C. Holm, and S. May, “Fraction of condensed counterions around a charged rod: comparison of Poisson–Boltzmann theory and computer simulations,” *Macromolecules* **33**, 199–206 (2000).
- [13] M. Cha, S. Ro, and Y. W. Kim, “Rodlike counterions near charged cylinders: Counterion condensation and intercylinder interaction,” *Phys. Rev. Lett.* **121**, 058001 (2018).

- [14] C. Hyeon and D. Thirumalai, “Mechanical unfolding of RNA hairpins,” *Proc. Natl. Acad. Sci. U. S. A.* **102**, 6789–6794 (2005).
- [15] R. Behrouzi, J. H. Roh, J. D. Kilburn, R. M. Briber, and S. A. Woodson, “Cooperative tertiary interaction network guides RNA folding,” *Cell* **149**, 348–357 (2012).
- [16] J. D. Honeycutt and D. Thirumalai, “The nature of folded states of globular proteins,” *Biopolymers* **32**, 695–709 (1992).
- [17] P. L. Adams, M. R. Stahley, A. B. Kosek, J. Wang, and S. A. Strobel, “Crystal structure of a self-splicing group I intron with both exons,” *Nature* **430**, 45–50 (2004).
- [18] J. A. Aronovitz and D. R. Nelson, “Universal features of polymer shapes,” *Journal de physique* **47**, 1445–1456 (1986).
- [19] R. I. Dima and D. Thirumalai, “Asymmetry in the shapes of folded and denatured states of proteins,” *J. Phys. Chem. B* **108**, 6564–6570 (2004).
- [20] J. D. Honeycutt and D. Thirumalai, “Static properties of polymer chains in porous media,” *J. Chem. Phys.* **90**, 4542–19 (1989).
- [21] A. M. Soto, V. Misra, and D. E. Draper, “Tertiary structure of an RNA pseudoknot is stabilized by “diffuse” Mg^{2+} ions,” *Biochemistry* **46**, 2973–2983 (2007).
- [22] N. Lee and D. Thirumalai, “Dynamics of collapse of flexible polyelectrolytes in poor solvents,” *Macromolecules* **34**, 3446–3457 (2001).
- [23] M. Muthukumar, “Theory of counter-ion condensation on flexible polyelectrolytes: adsorption mechanism,” *J. Chem. Phys.* **120**, 9343–9350 (2004).
- [24] A. Chremos and J. F. Douglas, “Counter-ion distribution around flexible polyelectrolytes having different molecular architecture,” *Soft Matter* **12**, 2932–2941 (2016).
- [25] N. A. Denesyuk, N. Hori, and D. Thirumalai, “Molecular simulations of ion effects on the thermodynamics of RNA folding,” *J. Phys. Chem. B* **122**, 11860–11867 (2018).
- [26] R. L. Hayes, J. K. Noel, A. Mandic, P. C. Whitford, K. Y. Sanbonmatsu, U. Mohanty, and J. N. Onuchic, “Generalized Manning condensation model captures the RNA ion atmosphere,” *Phys. Rev. Lett.* **114**, 258105–258106 (2015).

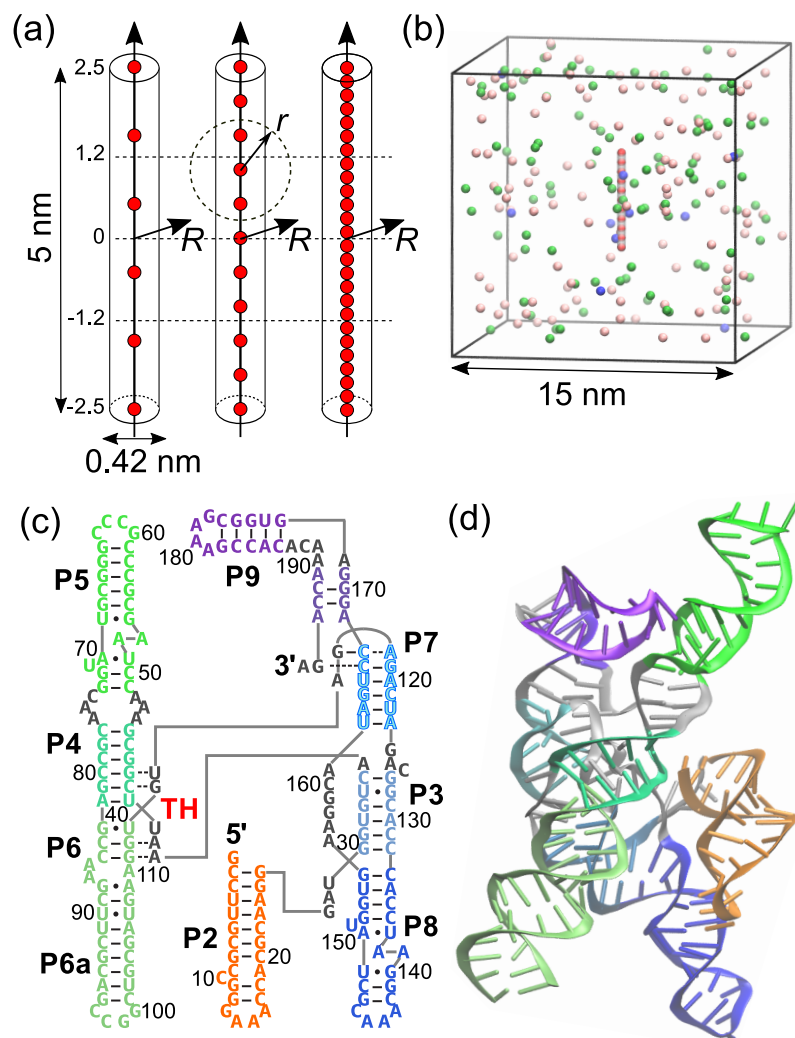


Figure 1. Schematic of charged rods and the *Azoarcus* ribozyme. **(a)** The dimensions of the rod, with aspect ratio 11.9, and positions of charges (in red) are illustrated. The diameter of the rod is 0.42 nm, which is the same as the diameter of the phosphate group in the coarse-grained RNA model. Negative charges are placed at regular interval with spacing that gives charge densities; $-1.0 e/\text{nm}$ (left), $-2.0 e/\text{nm}$ (middle), and $-5.0 e/\text{nm}$ (right). R is the radial distance in the cylindrical coordinate, whereas r represents the distance from the point charge to a position in space in the spherical coordinate. **(b)** A snapshot of the rod simulations. Ions are colored in blue for Mg^{2+} , green for K^+ , and pink for Cl^- . **(c, d)** The secondary (c) and tertiary (d) structures of *Azoarcus* group I intron ribozyme (PDB 1U6B [17]). The location of the triple helix (TH) is indicated on the secondary structure. The color codes in both the structures are the same.

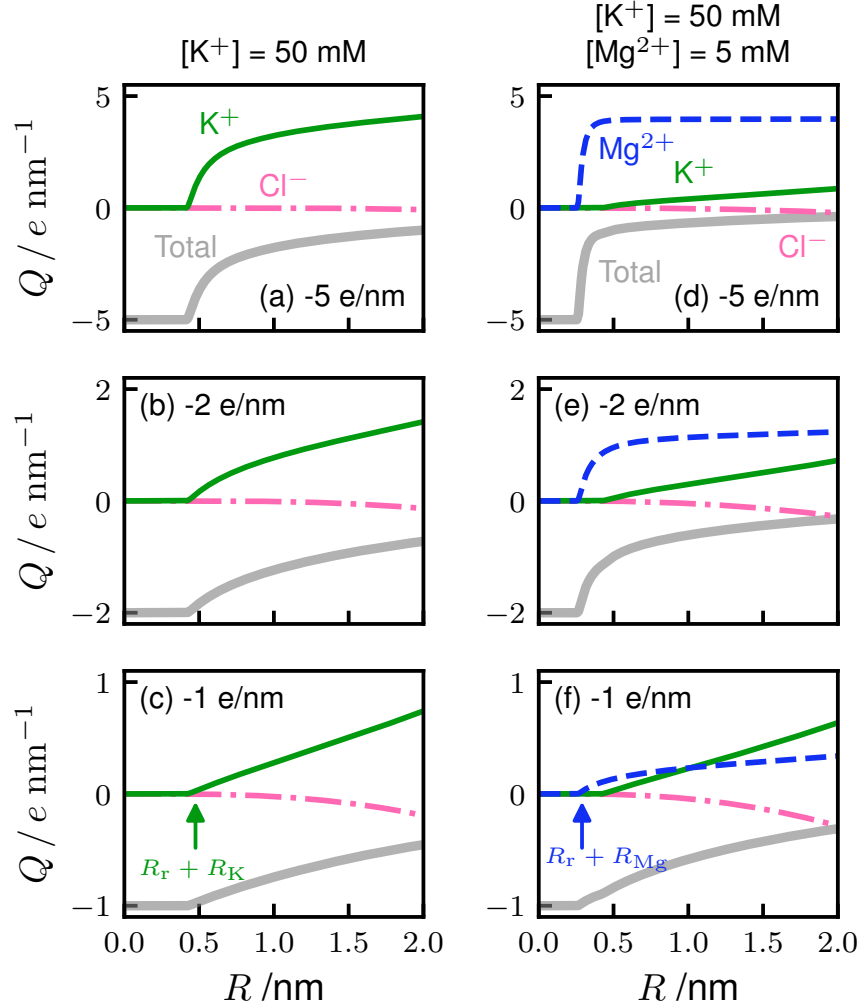


Figure 2. Comparison of the condensed ion species on charged rods with linear densities, $\rho_{1D} = -5 e/nm$ (top panels), $-2 e/nm$ (middle) and $-1 e/nm$ (bottom) in the absence (a-c) and presence (d-f) of Mg^{2+} . The cumulative charges per unit length Q (Eq. 7) is plotted as a function of R for contribution from each ionic species (annotated in the top panels). The total cumulative charge, $Q_T(R)$ (thick gray line), is the sum of charges of the rod and surrounding ions (Eq. 8). The solution conditions are indicated on the top. The ranges of exclusion by the volume interactions (Eq. 1), $R_r + R_K = 0.48$ nm for K^+ , and $R_r + R_{Mg} = 0.29$ nm for Mg^{2+} , are indicated by arrows in the bottom panels (R_r , R_K , R_{Mg} are radii of the rod, K^+ , and Mg^{2+} , respectively).

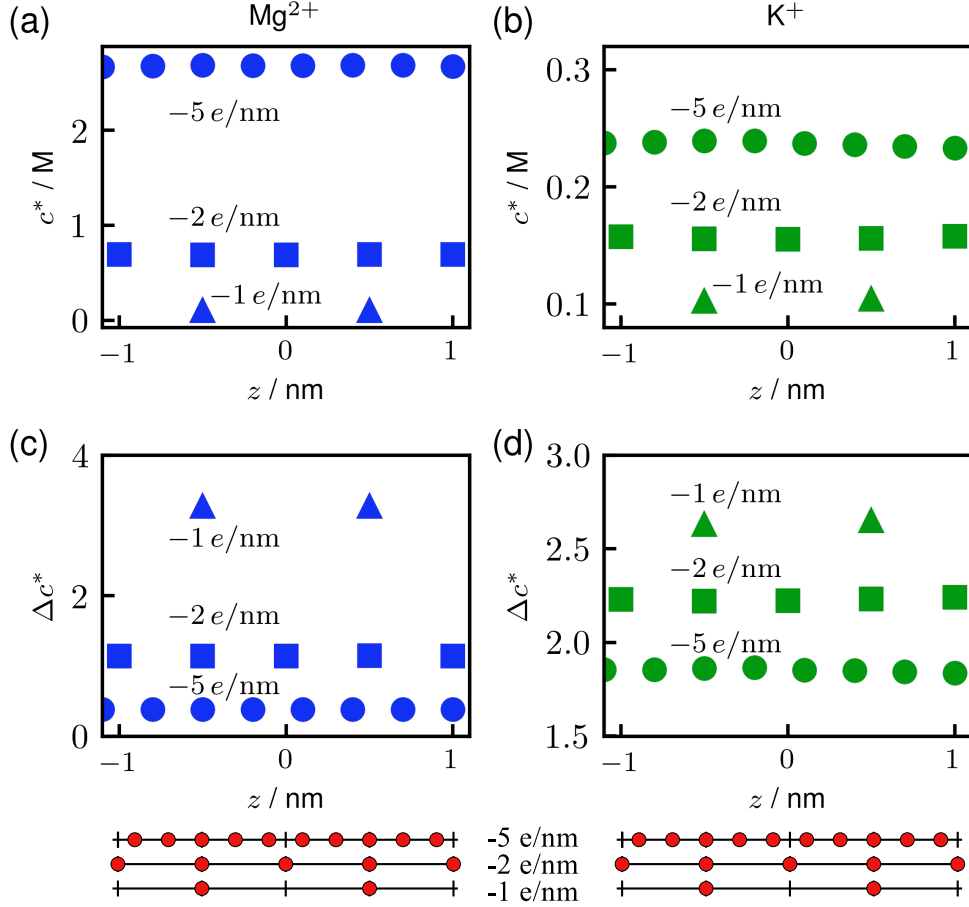


Figure 3. Condensation of Mg^{2+} (a, c) and K^+ (b, d) for the three rods with differing charge density, ρ_{1D} , (Fig. 1a) in 5 mM Mg^{2+} and 50 mM K^+ buffer. **(a, b)** Local ion concentrations of (a) Mg^{2+} and (b) K^+ . **(c, d)** Normalized fluctuations (Eq. 4) of the local ion concentrations of (c) Mg^{2+} and (d) K^+ at the same condition as in (a) and (b). The positions of negative charges on the three rods are indicated at the bottom. In order to avoid end effects, only the middle region of the rod ($-1.1 \text{ nm} \leq z \leq 1.1 \text{ nm}$) was used in the analysis.

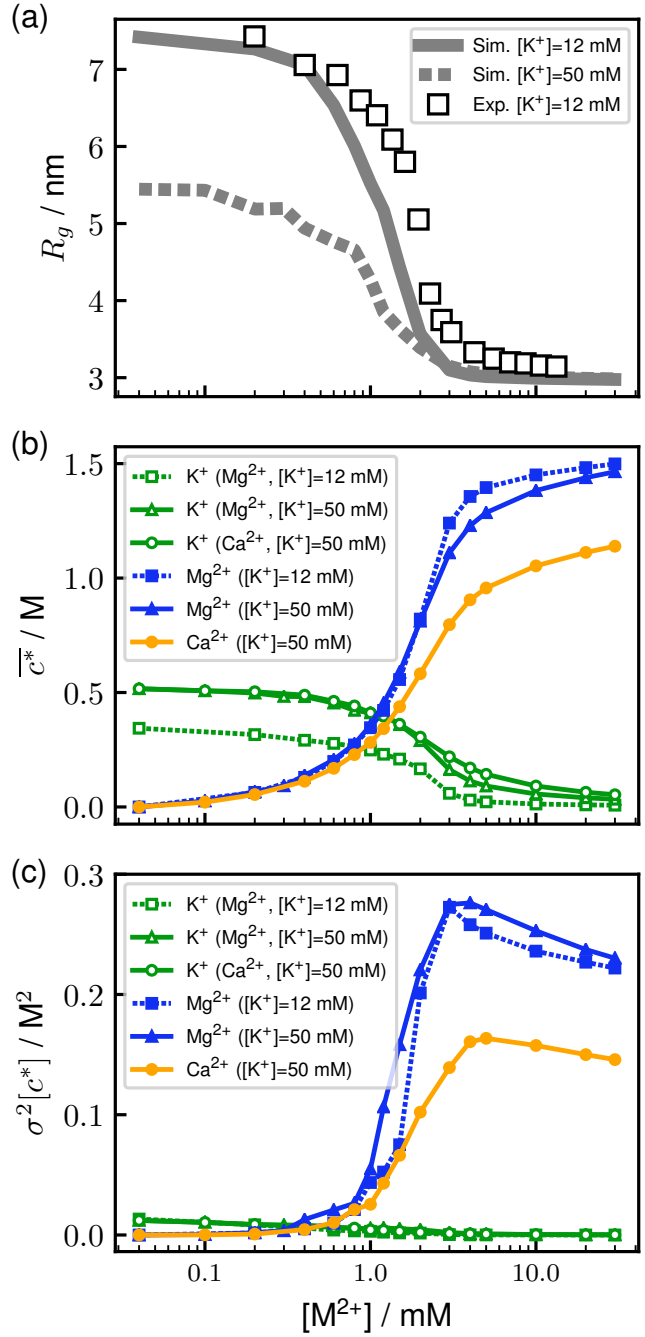


Figure 4. Ribozyme folding and ion condensation as a function of Mg^{2+} concentration. **(a)** Average radius of gyration (R_g) as a function of concentration of Mg^{2+} , that indicates the global compaction around the midpoint of $[Mg^{2+}] \sim 1.5 \text{ mM}$. Squares are experimentally measured R_g in a Tris buffer containing $12 \text{ mM } K^+$ taken from [15]. **(b)** $[Mg^{2+}]$ -dependence of local ion concentrations averaged over the nucleotide sequence, \bar{c}^* , for K^+ , Mg^{2+} and Ca^{2+} . **(c)** Variances in the concentrations along the RNA sequence, σ^2 .

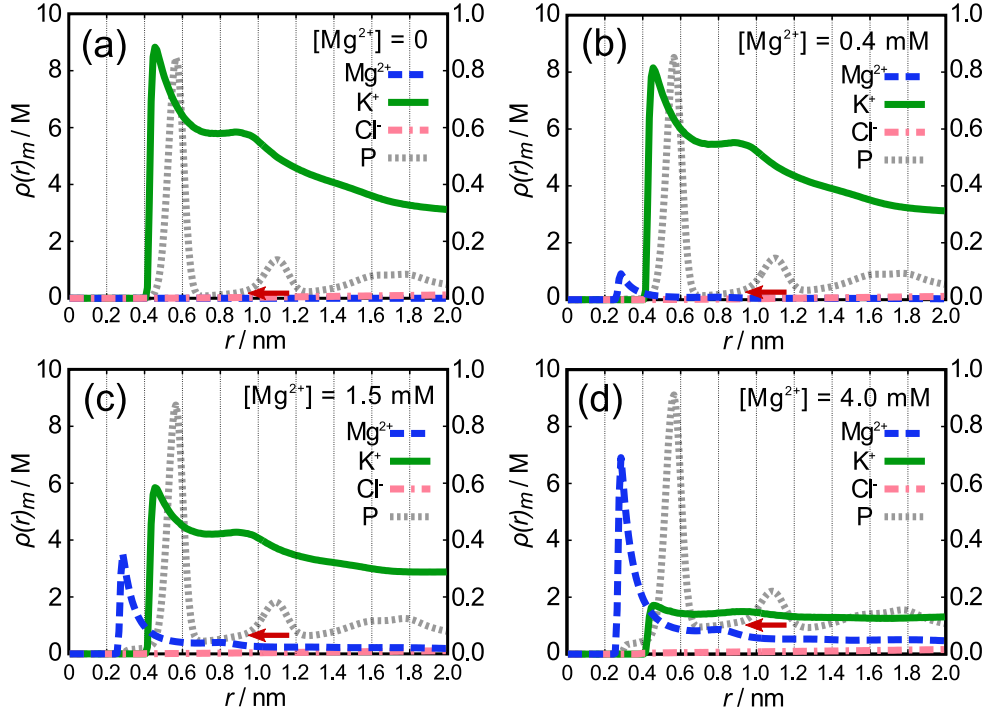


Figure 5. Radial profiles of ion distributions around the ribozyme, $\rho(r)$, for Mg^{2+} , K^+ , Cl^- , and phosphate (P) at various Mg^{2+} concentrations: (a) 0, (b) 0.4 mM, (c) 1.5 mM, and (d) 4.0 mM. The concentration of K^+ is 50 mM. Appropriate amount of Cl^- were added to the solution for the electroneutrality. Note that the scale for $\rho_{\text{Mg}^{2+}}$ and ρ_{P} (left axis) is 10 times greater than ρ_{K^+} and ρ_{Cl^-} (right axis). It should be pointed out that the density profile for K^+ decreases substantially as $[\text{Mg}^{2+}]$ increases. The red arrows indicate the amplitude of non-neighboring phosphates. The results in 50 mM KCl are shown in Fig. S1 in the SI. The density profiles for Mg^{2+} and P are roughly independent of the K^+ concentration.

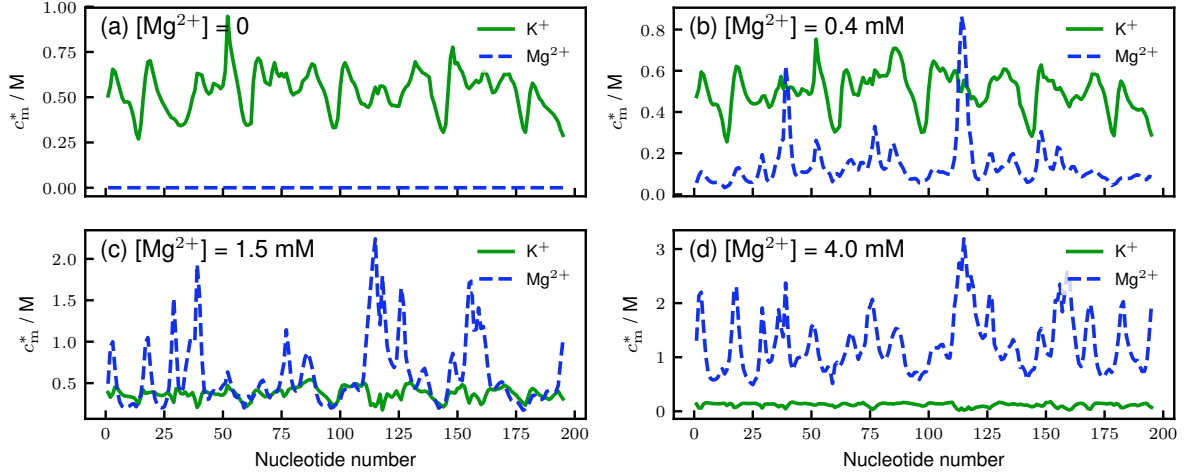


Figure 6. Fingerprint of ion coordination expressed as a local ion concentrations, c_i^* (i is the nucleotide position), for Mg^{2+} (blue) and K^+ (green). The local ion concentrations are calculated as the molarity of ions in the vicinity of each nucleotide ($r \leq \ell_B = 0.73 \text{ nm}$). The peaks with varying heights at different nucleotides positions as ribozyme folds reflects the architecture of the folded state. Most importantly, c^* is not uniform but varies dramatically along the nucleotides, which is very different from what is found for charged rods (see Fig. 3a). The results at 50 mM K^+ are shown in Fig. S2 in the SI.

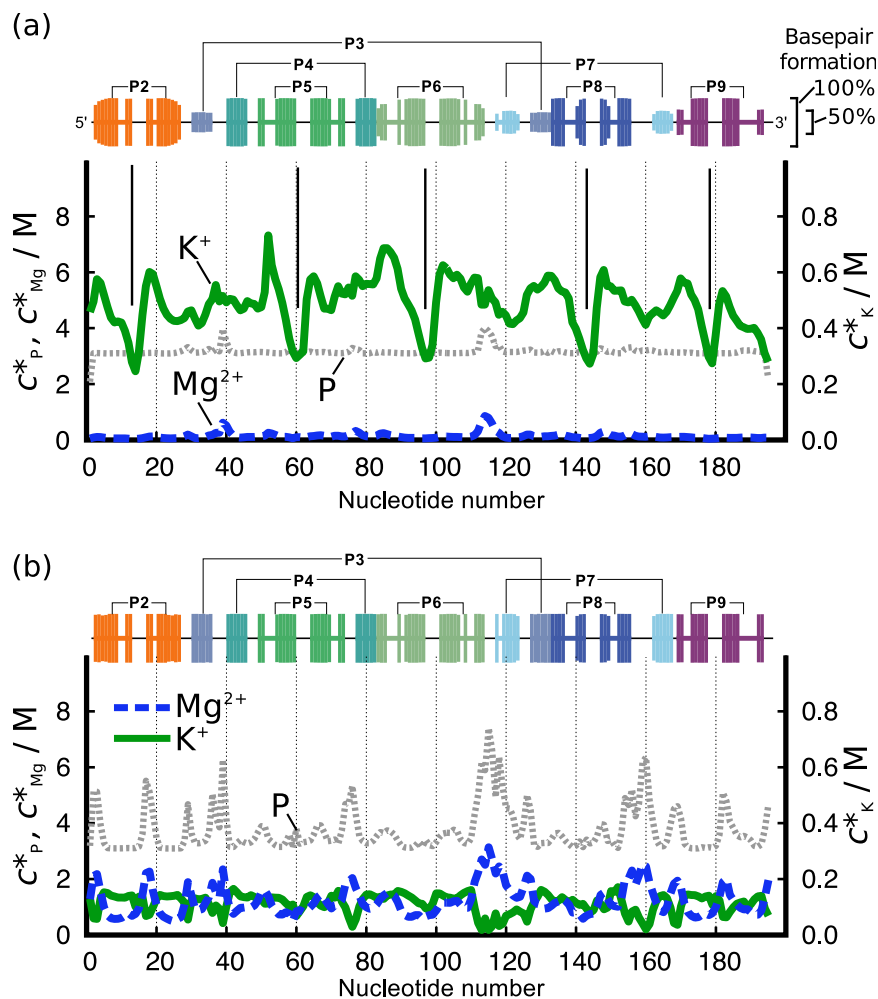


Figure 7. Relationship between K^+ condensation and residual structure. The fraction of secondary structure formation is shown on top as bars for each nucleotide. **(a)** At 0.4 mM Mg^{2+} , the profile of condensed K^+ (green) has several characteristic minima that correspond to loops in the stem-loop structures of P2, P5, P6, P8 and P9 (indicated by vertical black lines). See Fig. 1 for the structures. **(b)** At 4.0 mM Mg^{2+} , the profile of condensed Mg^{2+} correlates with the profile of phosphate (gray dashed). Such a correlation does not exist at low Mg^{2+} concentration. The secondary structures (various colored bars on top) are nearly fully formed.

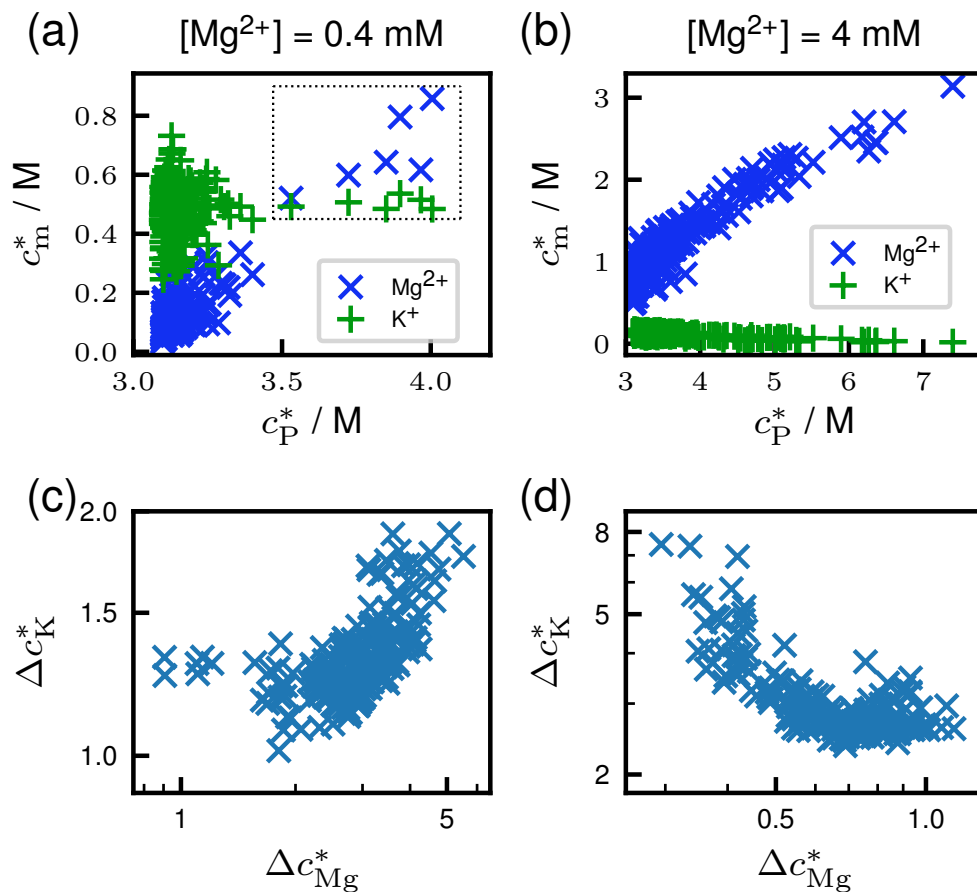


Figure 8. **(a, b)** Correlation between local ion concentrations of phosphate (c_P^*) and the cations (c_m^*) where m is either K^+ or Mg^{2+} . Each data point represents one nucleotide. There are 195 such data points in each panel. The solution conditions are (a) $[Mg^{2+}] = 0.4$ mM, and (b) 4 mM, both in 50 mM KCl. In (a), the data points at $c_P^* > 3.5$ M correspond nucleotides 39, 40, and 113-116 (inside the dotted rectangle), that are involving the tertiary helix. **(c, d)** Correlations of fluctuations, Δc^* , between Mg^{2+} and K^+ at (c) $[Mg^{2+}] = 0.4$ mM and (d) 4.0 mM in 50 mM KCl.

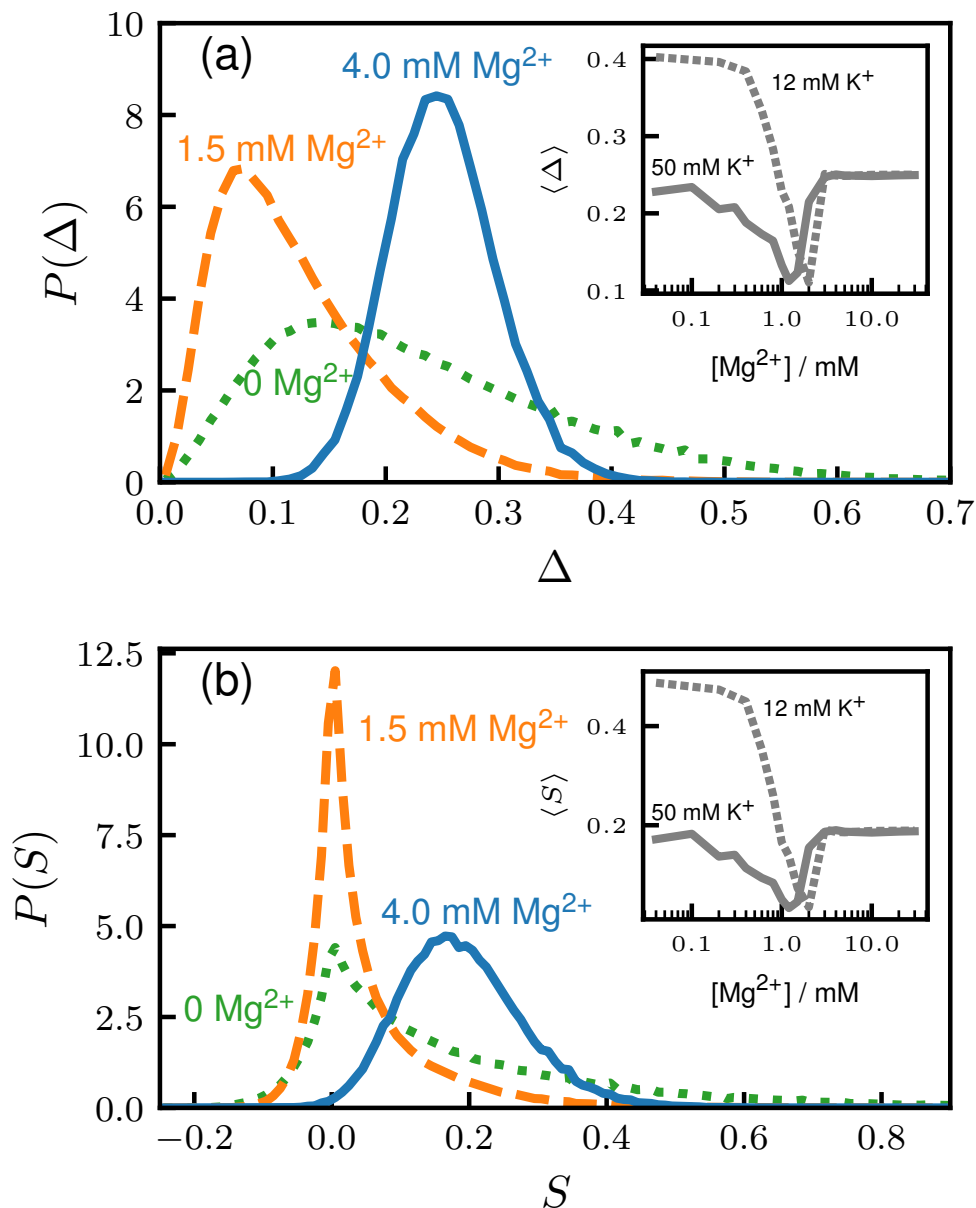


Figure 9. Probability distributions of shape parameters, (a) asphericity Δ and (b) prolateness S , for the *Azoarcus* ribozyme at three Mg^{2+} concentrations, 0 mM (dotted green), 1.5 mM (dashed orange), and 4 mM (solid blue). If the shape is a perfect sphere then $\Delta = S = 0$, whereas a perfect rod corresponds to $\Delta = S = 1$. The inset show the average values of $\langle \Delta \rangle$ and $\langle S \rangle$ as a function of $[Mg^{2+}]$ at $[K^+] = 12$ mM (dotted line) and 50 mM (solid line). The values of $\langle \Delta \rangle$ and $\langle S \rangle$ in the folded states are 0.24 and 0.17, respectively. Globally the shape of this ribozyme corresponds to a prolate ellipsoid.

SUPPORTING INFORMATION FOR “ION CONDENSATION ONTO RIBOZYME
IS SITE-SPECIFIC AND FOLD-DEPENDENT”

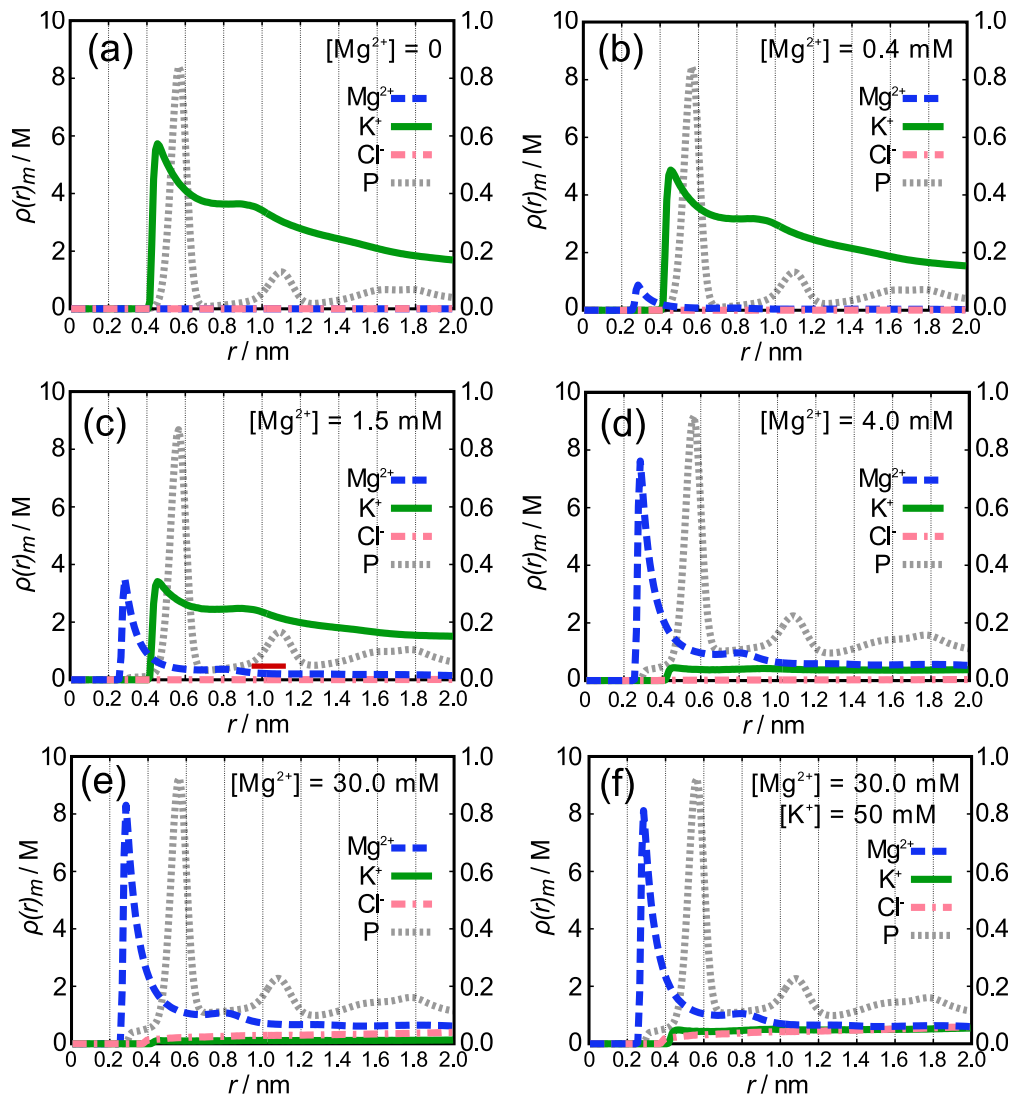


Figure S1: Radial profiles of local ion concentration, $\rho(r)$, for Mg^{2+} , K^+ , Cl^- , and phosphate (P) at $[\text{K}^+] = 12$ mM and various $[\text{Mg}^{2+}]$: (a) 0, (b) 0.4 mM, (c) 1.5 mM, (d) 4.0 mM, and (e) 30 mM. (f) The profile at $[\text{K}^+] = 50$ mM and $[\text{Mg}^{2+}] = 30$ mM. Appropriate amount of Cl^- were added to the solution for the electroneutrality. Note that the scale for $\rho_{\text{Mg}^{2+}}$ and ρ_{P} (left axis) is 10 times greater than ρ_{K^+} and ρ_{Cl^-} (right axis).

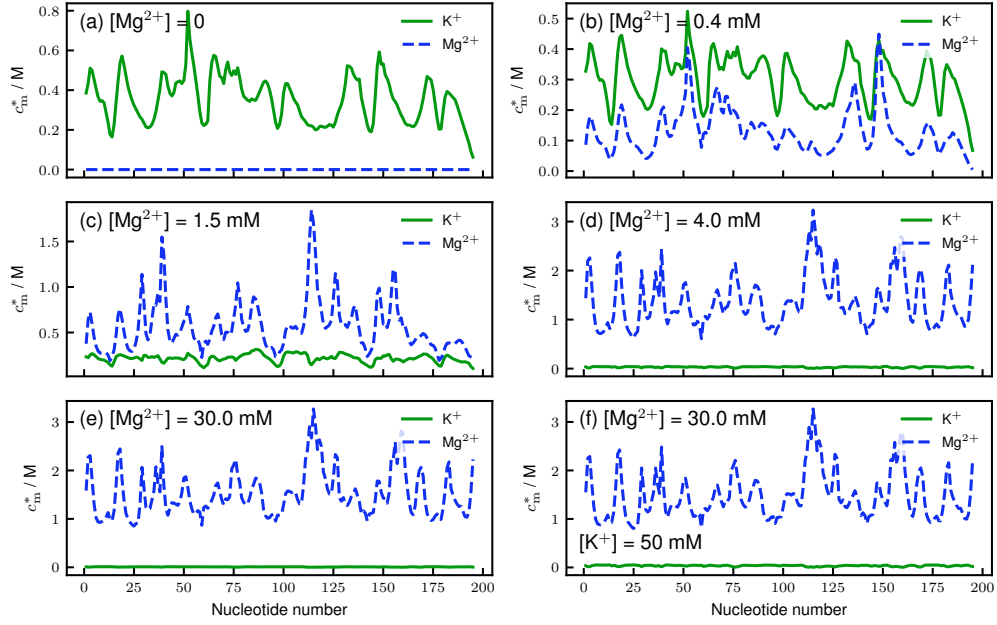


Figure S2: Local ion concentrations, c_i^* (i is the nucleotide position), for Mg^{2+} (blue) and K^+ (green) at $[\text{K}^+] = 12$ mM and various $[\text{Mg}^{2+}]$: (a) 0, (b) 0.4 mM, (c) 1.5 mM, (d) 4.0 mM, and (e) 30 mM. (f) The profile at $[\text{K}^+] = 50$ mM and $[\text{Mg}^{2+}] = 30$ mM.

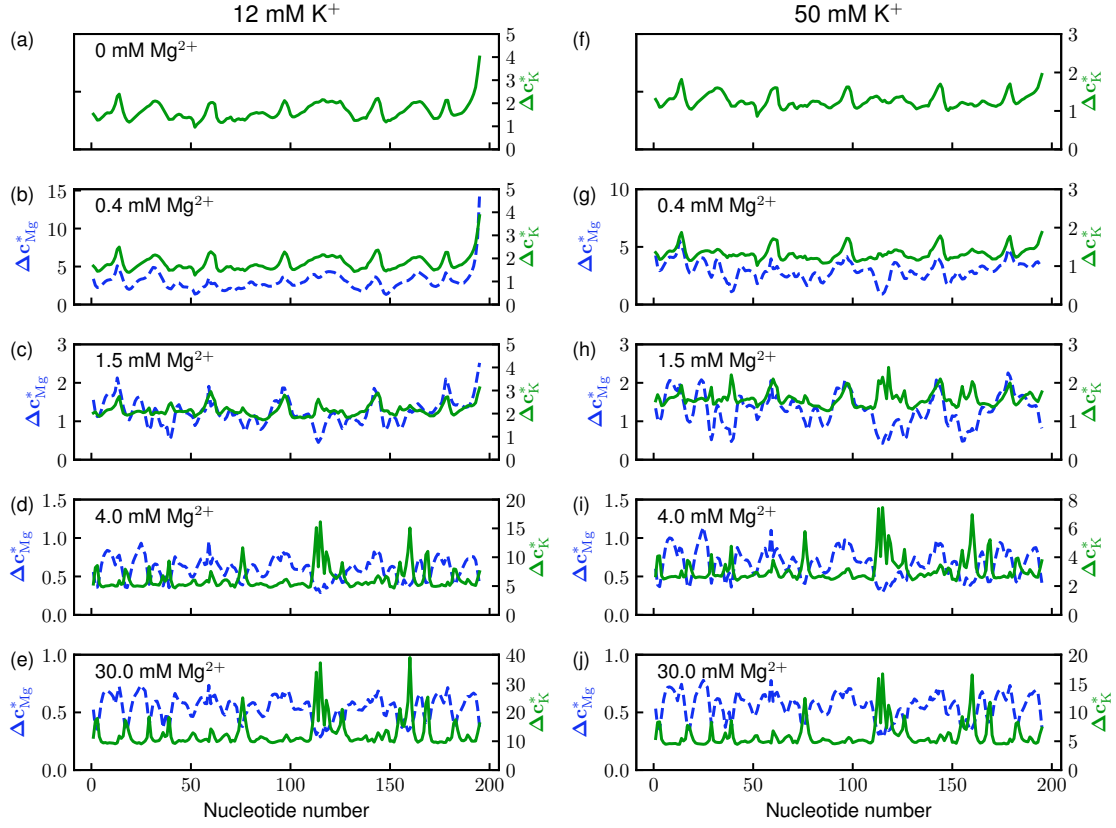


Figure S3: Normalized fluctuations of local ion concentrations, Δc^* (Eq. 4), for Mg^{2+} (dotted blue) and K^+ (solid green), in 12 mM KCl (left column; a–e) and 50 mM KCl (right column; f–j).

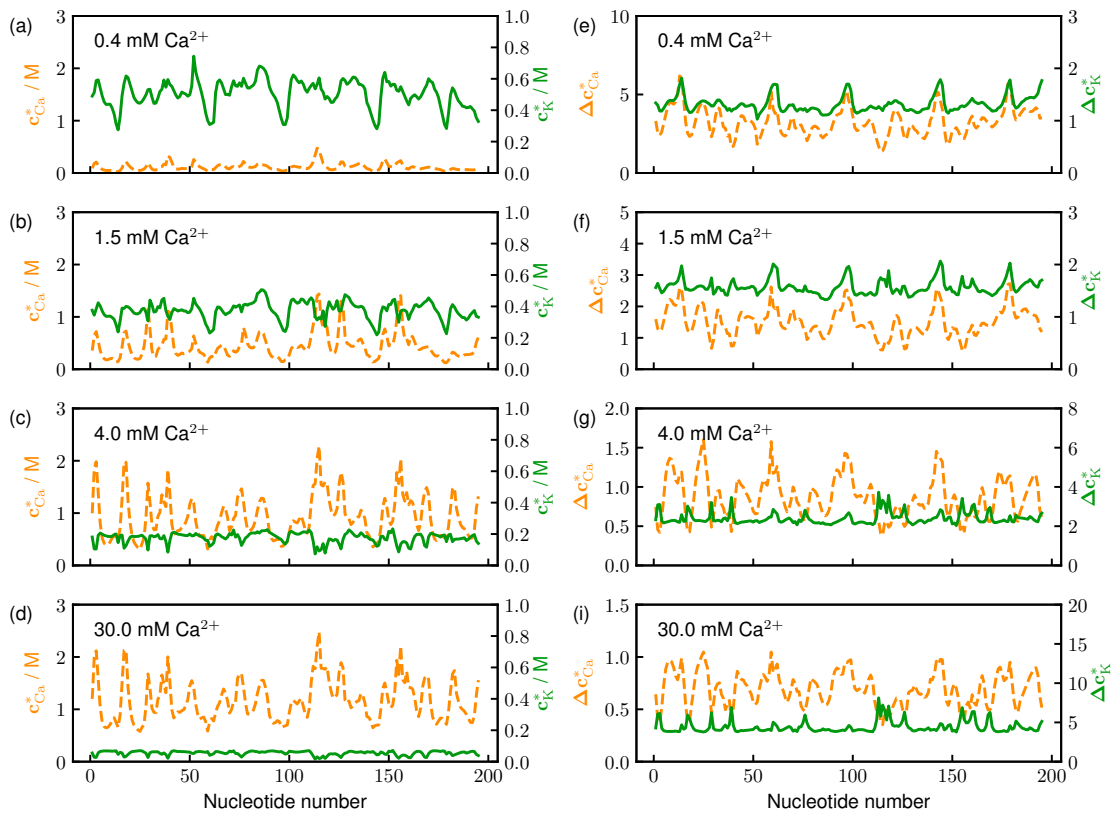


Figure S4: Sequence dependence of the local ion concentration (left column, c^*) and its fluctuations (right column, Δc^*) in the presence of Ca^{2+} ions instead of Mg^{2+} . The concentration of Ca^{2+} is labeled in each panel. $[\text{KCl}]$ is fixed at 50 mM.

Table S1: Parameters for excluded volume and electrostatic interactions.

Bead type	R_i/nm^*	$\varepsilon_i/\text{kcal mol}^{-1}$	z_i/e
Phosphate	0.21	0.2	-1
Rod charge	0.21	0.2	-1
Sugar	0.29	0.2	0
Base A	0.28	0.2	0
Base G	0.30	0.2	0
Base C	0.27	0.2	0
Base U	0.27	0.2	0
Mg ²⁺	0.08	0.9	2
Ca ²⁺	0.17	0.5	2
Cl ⁻	0.19	0.3	-1
K ⁺	0.27	0.0003	1

* If both interacting sites are RNA sites, we take $R_i + R_j = 0.32$ nm.